Proc. Estonian Acad. Sci. Eng., 2006, **12**, 3-2, 262–283

Accuracy of numerical methods by calculating static and quasistatic electric fields

Rauno Gordon[a], Tuukka Arola[b], Katrina Wendel[b], Outi Ryynanen[b] and Jari Hyttinen[b]

[a] Institute of Electronics, Tallinn University of Technology, Ehitajate tee 5, 19086 Tallinn, Estonia; rauno@elin.ttu.ee
[b] Ragnar Granit Institute, Tampere University of Technology, Biokatu 6, P.O. Box 692, FIN-33101 Tampere, Finland; tuukka.arola@tut.fi

Received 7 June 2006, in revised form 31 July 2006

Abstract. We study accuracy of numerical methods such as the Finite Difference Method (FDM) and the Finite Element Method (FEM) in calculation of electric fields inside the spherical conductor. Two different FDM formulations are described. Performance of these FDM formulations is compared to the analytical solution and FEM in models of an homogeneous sphere and three-layer spherical head. Electrodes were applied onto the surfaces on two opposite sides of the sphere. The FDM formulations were accurate to within 5% inside the object but errors increased to 15% near tissue boundaries of the three-layer model that were close to the electrodes. Differences between calculation methods at the electrode location reached 25% in some cases.

Key words: biomedical engineering, bioimpedance, potential distribution, lead field, FDM, FEM.

1. INTRODUCTION

In this article we investigate the accuracy of FDM and FEM in calculation of electric fields, e.g. for simulation of bioelectric fields [1,2] or for bioimpedance measurement [3]. These methods can be used also for simulation in any electrical conductance scenario. Our interest is in validating the numerical methods in calculating electrical potential and current distribution in biological objects such as the human head (EEG – Electroencephalography, EIT – Electrical Impedance Tomography), thorax (ECG – Electrocardiography, EIT) and heart (ICG – Impedance Cardiography). We analyse more closely the performance of numerical methods near the current insertion electrodes. That makes our results applicable for bioimpedance simulation and impedance tomography [4].

Electroencephalography as well as bioimpedance measurement in the human head have been used for the localization of active regions in the brain [5–7]. The EEG measures directly the electric activity of the brain and bioimpedance measures the changes in electric conductance. Regions in the brain with higher activity need more oxygen, and blood supply in these regions is increased. Active regions in the brain become more conductive because blood is a better electric conductor than the white or gray matter of the brain. Identification of the active region can more reliably be done with functional Magnetic Resonance Imaging (fMRI). Alternatively the bioimpedance measurement gives reliable results with relatively cheap equipment that is portable and can be used in case of medical emergency. Bioimpedance measurement on the head (EIT on the head) uses electrodes on the head surface to generate and measure the electric field and therefore measures non-invasively.

Measurement of the heart bioimpedance can also be done non-invasively with an electrode array on the body surface (EIT on thorax). The objective is to get information on the cardiac blood output and also on the muscle condition. In the case of the heart we are also interested in invasive measurement that uses electrodes inside the heart chambers. Invasive measurement can be conducted by intracardiac catheter that is inserted to the left or right side of the heart through veins. One catheter wire can carry several electrodes. Those electrodes have to insert the current and also measure the potentials. In addition, in many cases the intracardiac catheter also has to submit a pacing or defibrillation pulse when used by an implanted cardiac pacemaker or defibrillator. The implantable nature of the cardiac pacemaker complicates the impedance measurement process and limits considerably the number of usable electrodes.

Until now we have been content with the results of FDM calculations and taken them as a practical way to observe signals as relative numbers. This study was initiated by the growing need to be able to get absolute signal values from simulations. As the simulated signal values are actually comparable with the physically measured ones, simulation of bioelectric phenomena becomes more useful. We compare potential distributions, calculated inside a homogeneous sphere, with four methods: analytical formula, FEM solver and FDM in two different formulations. Similar validation of the computation methods is described in [8–11].

2. NUMERICAL METHODS FOR SIMULATING BIOELECTRIC PHENOMENA

Mathematical equations, including integrals and derivatives, cannot be implemented on computers without approximation. In some situations, integral equations can be converted to differential equations and vice versa. There are numerical methods for solving them both. Bioelectric simulation of the human body leads essentially to solving the Laplace and Poisson equations [12,13] for current conduction in a volume conductor.

2.1. Model geometry

We have used numerical methods to calculate electrical potential distribution in a three-dimensional model of a sphere with a radius of 5 cm and electric conductivity of the blood $\sigma = 0.7$ S/m. Electrodes were placed on two sides of the sphere on the surface. The source current was fixed at 1A in all cases.

For demonstration we also compute the potential distribution in the three-layer spherical head model. We chose this particular model because the analytical formula is also capable of solving it. The three-layer model gives us the opportunity to observe the performance of the solvers in a scenario that is closer to real application. The outer radius of the head sphere is $r = 9.2$ cm. The scalp layer thickness is 7 mm and scull layer thickness 5 mm. The conductivity of the brain is 0.45, of the skull 0.03 and of the scalp 0.45 S/m. The conductivities of the scalp and the brain were the same as in [14,15], but the skull conductivity has been calculated from the skull/brain resistivity ratio of 15 [16]. The source current was fixed at 1A in all cases.

2.2. Analytical formulation

The analytical model we used to compare our results with has been defined by Rush and Drisscoll [14]. It is capable of calculating potential distribution inside a conductive sphere model and can use an inhomogeneous model with up to 3 layers of different conductivities [14,17–20]. This model was created for solving electrical lead field problems of the head. In this model the electrode size is not specified, it uses point electrodes instead. The model allows to use two electrodes, which may be located anywhere on the sphere surface. We use a configuration of the electrodes that are on two opposite sides of the sphere. We use this analytical model to obtain the potential distribution inside a homogeneous sphere and in a three-layer spherical head model.

2.3. Discrete formulation

The equations are discretized by using FEM or FDM. The discretization of the equations result in a set of linear equations that can be represented as sparse matrices

$$Ax = b, \tag{1}$$

where A is a symmetrical and positive definite $n \times n$ matrix (n being the number of elements). There are various methods to solve a set of linear equations such as Eq. (1). However, the size and sparsity of the matrices encountered in bioelectric simulation of the human body make most of the methods obsolete. In such cases we must use iterative methods. In iterative methods the vector x is modified in such a way that the difference between the left and the right hand side of the matrix equation is minimized. The vector x is modified between each iteration and when the difference becomes small enough, the problem is

considered to have been solved. There are various ways of approximating the modification of x [21,22]. One of the most effective and most used iterative methods is the Conjugate Gradient (CG) Method. We have also used CG to solve our matrix equations. It is generally formulated as

$$\nabla f(x) = Ax - b = 0, \tag{2}$$

with the iteration equation

$$x^{k+1} = x^k + \alpha_k p^k. \tag{3}$$

These equations state that the minimum of the error function $f(x)$ can be found at a point where the gradient of the function is zero. Effectively, by minimizing the function $f(x)$ the equation $Ax = b$ can be solved. Also the coefficient α_k is to be chosen so that $f(x^{k+1})$ is minimized and the optimization directions p^k are to be chosen so that they are conjugated with the matrix A, i.e. $(p^i, Ap^j) = 0$ as $i \neq j$ [23].

The convergence of the CG depends on the spectrum of eigenvalues of the matrix A and it can be improved by *preconditioning*. With preconditioning the equation to be solved becomes

$$P^{-1}Ax = P^{-1}b, \tag{4}$$

which is equivalent to the original equation but is better suitable for iterative solution. The choice of the preconditioner P^{-1} is all but trivial and depends on the problem at hand, its size and complexity. We have used diagonal and in-place incomplete Cholesky preconditioners [23] depending on the size of the problem.

In order to select a suitable preconditioner, one has to consider the complexity of time and memory the preconditioner can have. For large problems, where memory size becomes a limit, simple preconditioners such as the diagonal is used. Generally, more complex preconditioners perform better and drastically reduce the iterations needed for the solution to converge. The bigger the problem, the better preconditioner it requires. Unfortunately, better preconditioners can rarely be used for large problems due to memory constraints.

2.4. The finite difference method

In bioelectromagnetic simulations of the human body we want to calculate the current and potential distribution in a model. The model can be constructed by creating a general model of the area of interest or by extracting it from medical images. As computer performance and memory capacity increase, even bigger and more complex models can be generated and used for simulation. Thus now it is possible to create realistic models from e.g. magnetic resonance (MR) or computed tomography (CT) image sets.

The bioelectric potential field in the volume Ω can be defined with the Poisson equation

$$\nabla \cdot \sigma \nabla \varphi = \nabla \cdot J_S \qquad \text{in } \Omega, \tag{5}$$

where σ is conductivity, φ denotes the potential and J_S is current source density. For piecewise homogeneous media, Eq. (5) can be rewritten as

$$\sigma \nabla^2 \varphi = \nabla \cdot J_S. \tag{6}$$

Now, using Taylor series expansion, the second order derivative can be defined as

$$\frac{\partial^2 f(x)}{\partial x^2} = \frac{f(x+\mathrm{d}x) + f(x-\mathrm{d}x) - 2f(x)}{\mathrm{d}x^2}. \tag{7}$$

Substituting the Taylor series expansion of the second order derivative (7) to (6) and discretizing the result into piecewise linear cubic subvolumes, we get for node k

$$\varphi_k \sum\nolimits_n G_n - \sum\nolimits_n \varphi_n G_n = i_k, \tag{8}$$

where φ_n is the voltage at the neighbour, G_n is the conductance to the neighbour, φ_k is the voltage at node k and i_k is the input current at the node k. For sourceless nodes, $i_k = 0$. Applying Eq. (8) for all nodes in the model, a set of simultaneous equations is obtained, which can be formulated as a linear matrix equation

$$Ax = b.$$

The matrix A contains conductances between nodes, x is the result and b is the current source vector.

2.5. The finite element method

Whereas in FDM the solution is approximated by replacing the second order derivatives with discrete versions, in FEM the idea is to approximate the solution with a set of basis functions and with their linear combinations. The result is obtained from the boundary conditions for the problem. In FEM the problem is transformed into weak formulation and approximated by the Galerkin method. The model domain can be divided into small subdomains, i.e. elements in which the solution is approximated by a linear combination of basis functions belonging to a Hilbert space H. Notation a(·,·) is used for a bounded bilinear form $H \times H$ into R. The variational problem is to find $u \in H$, such that

$$a(u, v) = F(v) \quad \text{for all} \quad v \in H, \tag{9}$$

where u and v are arbitrary functions, a is a mapping function and F is a functional, belonging to H^*, the dual space of H.

If we define a finite dimensional subspace H_h of H such that $u_h \in H_h$, Eq. (9) becomes

$$a(u_h, v_h) = F(v_h) \quad \text{for all} \quad v_h \in H_h, \tag{10}$$

which is called the finite element method. The full mathematical background of this method is complicated [24]. The result of the formulation is a linear equation

$$Ax = b.$$

The basis functions φ_i are usually chosen to be low-order polynomials and belong to subspace $\{\varphi_1, \varphi_2, \ldots, \varphi_n\}$ of H_n. Now, a discrete version of Eq. (10) is

$$A(u_n, v) = F(v) \quad \text{for every} \quad v \in H_n. \tag{11}$$

By choosing $u_n = \sum_{i=1}^{n} \alpha_i \varphi_i(x)$, we get

$$\sum_{i=1}^{n} \alpha_i a(\varphi_i, \varphi_j) = F(\varphi_j) \quad \text{for every} \quad j = 1, 2, \ldots, n, \tag{12}$$

which again can be represented as a linear matrix equation $Ax = b$. A commonly used technique is to select basis functions such that the majority of matrix A elements are

$$a_{ij} = a(\varphi_i, \varphi_j) = 0 \quad \text{if} \quad |i - j| \geq 2, \tag{13}$$

and for the right hand side of the matrix equation

$$(F_n)_i = F(\varphi_j). \tag{14}$$

The basis functions are selected in such manner that all the elements attached to a node have the same value at the node. It is also required that the values of the first derivatives of the basis functions are the same at the node. By requiring the basis functions to be zero at all other points x_j except the point in question x_i as in Eq. (13), one gets a really sparse matrix A, since all but neighbouring nodes have a value of zero. The more nodes are used, the higher order polynomials can be used to approximate the solution [21].

2.6. Choice of the FDM grid

In FDM, there is a couple of ways to choose subvolumes, i.e. the discretization grid and the nodes that form the grid. Different formulations determine how the conductance between nodes is calculated. Due to the digitization of medical images, a realistically shaped volume conductor consists of voxels. Thus there are two obvious ways of defining the node spacing and also the conductance between two nodes: the first one places the nodes in the middle of each voxel (centre-voxel) and the second one has nodes placed in the vertices of each voxel (corner-voxel). This study examines both of these methods.

2.6.1. Corner-voxel formulation

In corner-voxel formulation the boundaries of volumes can be easily defined since the nodes are located at the surface of each voxel as seen in Fig. 1a. This formulation allows a voxel to be unambiguously defined as a specific material. On the other hand, the conductance between two nodes can not be easily determined and must be calculated using the conductivity of the material and the size of the neighbouring voxels as seen in Fig. 1b. Since the nodes in the grid do not correspond to a specific voxel in the original data, it might be difficult to relate the results and the voxels in the original model and in such case interpolation is needed. The corner-voxel formulation has been used, e.g., at the Ragnar Granit Institute at Tampere University of Technology [25,26].

Generally, the macroscopic conductance for a homogeneous volume conductor can be defined using Ohm's law. Additionally, by noting that in a linear resistor or conductor the electric field E is constant along the resistor axis, conductance can be defined as

$$G = \frac{\iint J\mathrm{d}a}{\int_L E\mathrm{d}l} = \frac{\sigma \iint E\mathrm{d}a}{\int_L E\mathrm{d}l} = \frac{\sigma A}{l} = \frac{I}{U}, \tag{15}$$

where A is the cross-section area of the conductor and l is the length of it. The total resistance between two adjacent nodes can be calculated as a parallel sum of four resistors from the four adjacent voxels. Each of the resistors occupies one quarter of the voxel as it can be thought to be the effective media the resistor

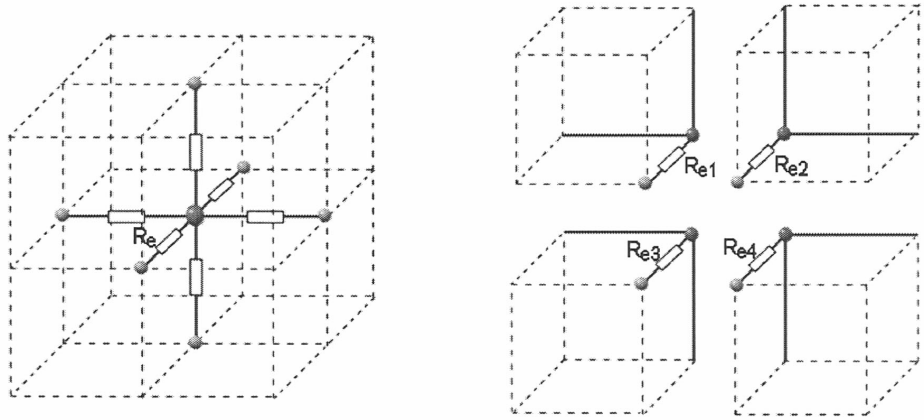

(a) (b)

Fig. 1. Node definition in the formulation where nodes are inserted to the vertices of each voxel; the resistance between two adjacent nodes is calculated as a parallel circuit of resistors, formed by the adjacent volumes: (a) the grid spacing with respect to the voxels in the data; (b) the components of a resistor between two adjacent nodes.

represents. Thus the formula to calculate the conductance between two nodes becomes

$$G = \frac{\sigma_1 A_1 + \sigma_2 A_2 + \sigma_3 A_3 + \sigma_4 A_4}{4l}, \tag{16}$$

where A_i $(i = 1,2,3,4)$ is the voxel cross-section area in the direction of the neighbour and l is the distance to the neighbour. This is true for all nodes regardless of their location in the model and allows piecewise approximation of inhomogeneous conductivity.

2.6.2. Centre-voxel formulation

The formulation of FDM conductivity matrices as used at Tallinn University of Technology is based on the idea that one node of the mesh represents also one voxel of volume data. When electric current flows between the nodes, it effectively flows from the centre of the voxel to the centre of another (centre-voxel formulation, Fig. 2).

The conductance G between the nodes is defined by the formula

$$G = d \frac{1}{\frac{1}{2\sigma_1} + \frac{1}{2\sigma_2}}, \tag{17}$$

where d is the distance between two nodes (or voxel size) and σ_1 and σ_2 are electrical conductivities of the media at the locations of the nodes 1 and 2.

The original purpose behind this formulation of the FDM was to model implanted electrodes. Therefore it was a logical choice to implement electrodes of the size of one or more voxels that have a staighforward surface contact with the surrounding media.

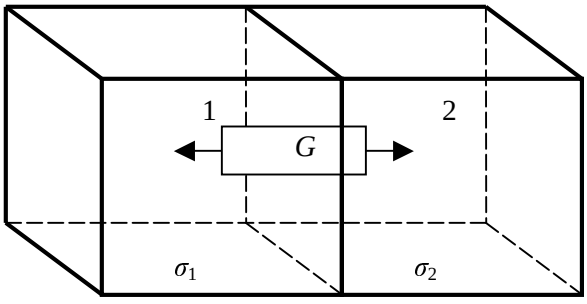

Fig. 2. FDM conductivity formulation with mesh nodes in the centre of the volume data voxels.

2.7. The sphere model used in FDM formulations

In both of the FDM formulations the same volume data model was used as a basis for FDM grid generation. Resolutions used for the FDM grid were 80, 100, 125, 150, 175, 200, 225 and 250 voxels of linear resolution for the sphere. The models were then modified in such a way that source and sink electodes were added as a layer of one or more voxels to the opposite sides of the sphere model. The outer limits of the model were cube shaped with identical number of voxels in *x*, *y* and *z* direction. The electrode layers effectively increased the model size by 2 voxel in each direction. The resulting model resolutions and the number of elements in FDM solver is found in Table 1. The basic electric field can be calculated with just one voxel electrode. Additionally bigger electrodes are implemented with more voxels used per electrode on the surface. The electrode shapes used and the corresponding circular electrodes are shown in Fig. 3. Volume data for the creation of FDM matrices was calculated using Matlab. Centre-voxel formulation matrices were created in Matlab and corner-voxel matrices using custom software on Java platform. Conjugate Gradient method was used to solve the matrices with Incomplete Cholesky preconditioning.

Table 1. Resolution of the FDM sphere model

Sphere resolution	Nodes in centre-voxel formulation	Nodes in corner-voxel formulation	Voxel size, mm	Average calculation time, min:sec
80^3	551 368	571 787	1.25	0:15
100^3	1 061 208	1 092 727	1.00	0:29
125^3	2 000 376	2 048 383	0.80	1:08
150^3	3 511 808	3 581 577	0.66	2:08
175^3	5 451 776	5 545 233	0.57	3:40
200^3	8 242 408	8 365 427	0.50	6:17
225^3	11 543 176	11 697 083	0.44	9:40
250^3	16 003 008	16 194 277	0.40	24:00

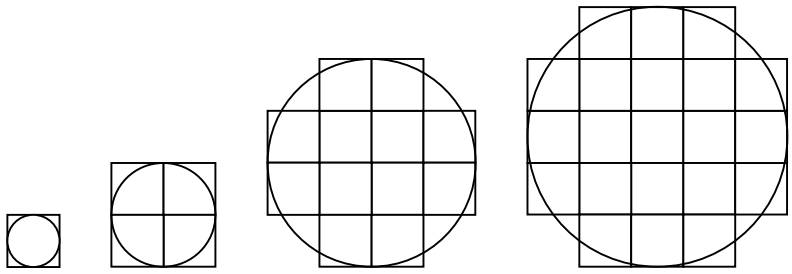

Fig. 3. Four different shapes used for FDM modelling of the electrodes; the number indicates the number of voxels used for modelling the circular electrode in the FDM model.

Diagonal preconditioner was used for the largest matrix with over 16×10^6 nodes (matrix rows and columns) to conserve memory. Matrices were solved with custom-built efficient Java-based solver on a PC with 2 GB of memory and a 3 GHz processor. The largest FDM problems used about 1.2 GB of memory. Calculation times of the linear systems can be found in Table 1.

2.8. The sphere model used in the FEM

The FEM model was created with two different mesh densities. The low-resolution mesh consisted of approximately 10 000 tetrahedral mesh elements and the high resolution mesh consisted of approximately 200 000 elements. The mesh was rebuilt for every electrode size. Electrodes with radii 0.25, 0.5, 1 and 2 mm were used for computing the potential distribution. Mesh density was increased around the electrode slightly in order to represent the contact area as accurately as possible. As the area around the electrode has the highest current density, increasing mesh density there should theoretically improve the accuracy of the solution and also the linear system solver convergence rate. Figure 4 depicts the low-resolution and high-resolution meshes. The electrodes with a radius of 0.25 mm are shown both at the low-resolution and the high-resolution mesh. Figure 5 shows that at low resolution the small electrode connection to the surface is depicted with only 4 elements and therefore should theoretically not provide better results than the low-resolution FDM. All FEM models, meshes and calculations were performed with the Femlab/Comsol software.

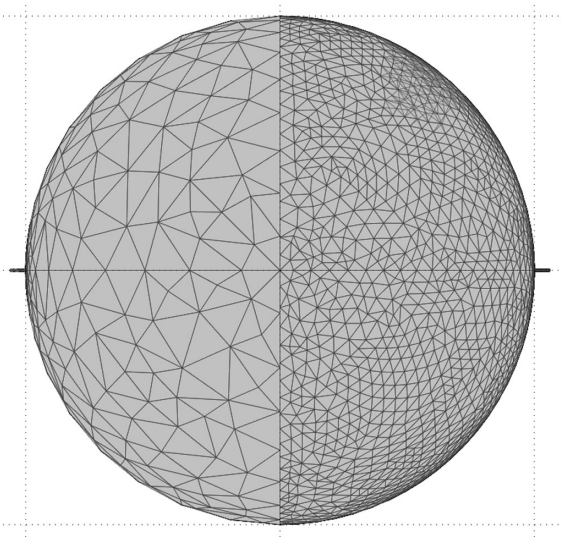

Fig. 4. FEM model mesh at low resolution with 10 000 elements (left half) and high resolution with 200 000 elements (right half).

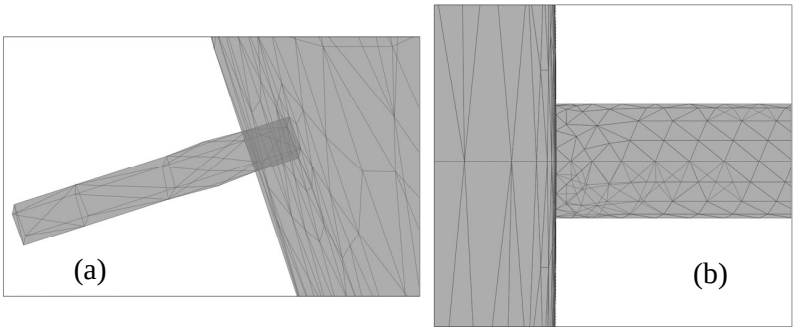

Fig. 5. FEM mesh near electrodes: (a) low-resolution mesh with electrode r = 0.25 mm; (b) high-resolution mesh with electrode r = 0.25 mm.

3. RESULTS

The computed results show the potential distribution inside the sphere model. The easiest way to present the potential distribution is to show a slice through the middle of the sphere with the potential shown gray-coded (Fig. 6). In order to make a clean cross-method comparison, we plotted only the potentials on the centre line through the sphere that also goes through the electrodes (Fig. 7).

Potential distribution inside the homogeneous sphere, computed with the analytical method, FDM and FEM look almost the same when plotted on the same large-scale drawing. To see the differences, we investigated a 1 cm deep area near the electrode (shown with a dashed box in Fig. 7).

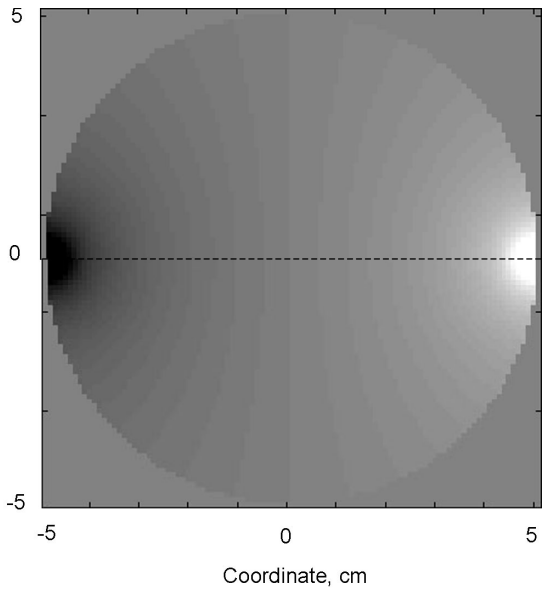

Fig. 6. Potential distribution on the centre slice inside the homogeneous sphere; analytical solution.

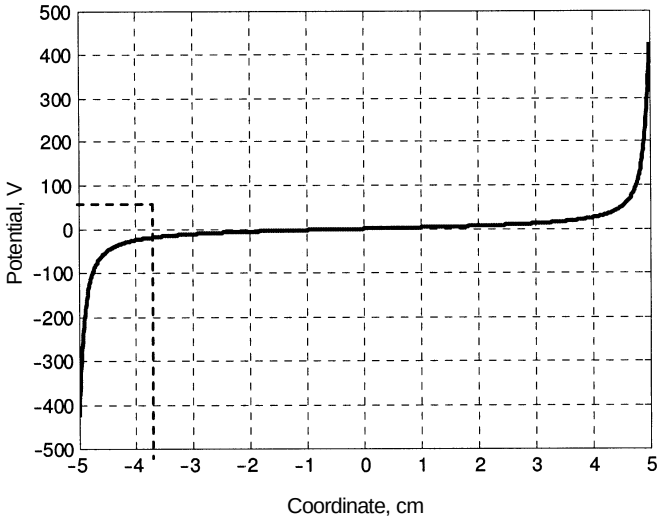

Fig. 7. Potential distribution on the middle line (dashed line in Fig. 6) between electrodes inside the homogeneous sphere; analytical solution.

Figure 8 shows that with a smaller electrode the potential between the two electrodes increases. One has to keep in mind that the current stays fixed at 1A

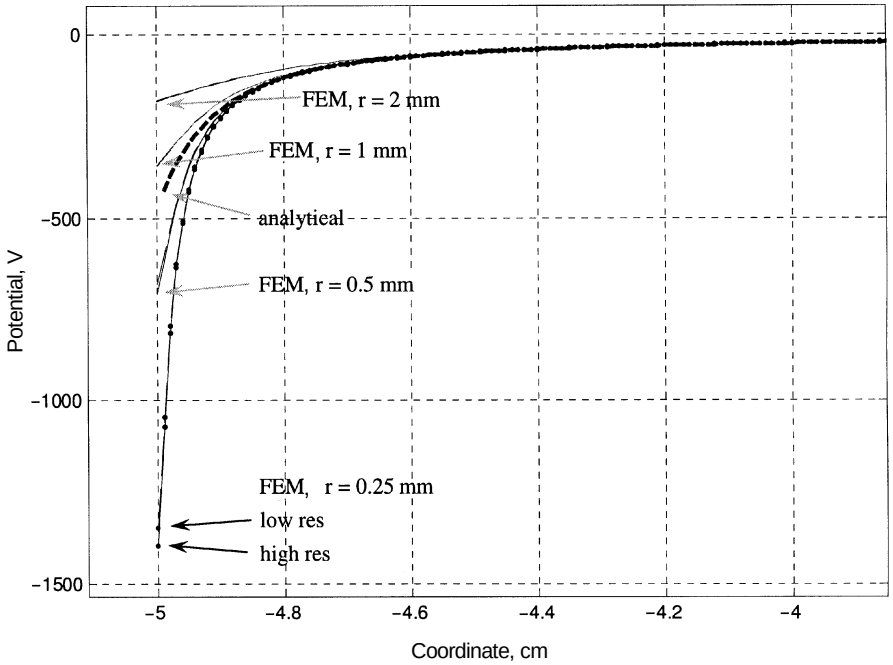

Fig. 8. Potential distribution on a line through the sphere near the surface on the left side of the sphere; electrode touches the sphere at the coordinate –5 cm.

and the potential distribution in the other half of the sphere is similar to the potential on the left side of the sphere as seen in Fig. 7. The FEM results differ from the analytical solution noticeably only near the electrode until the depth of 3 mm. Inside the rest of the sphere the analytical solution matches the FEM solution. It would be logical to conclude that when the electrode size diminishes, the potential needed to produce the same current approaches infinity. All the four electrode sizes plotted in Fig. 8 are presented with two lines: the solid line for the high resolution and the dashed line for the low resolution of the FEM mesh. It is noticeable that the low and high resolution lines are almost indistinguishable from each other. The biggest difference between the solutions with low and high resolution occurred in the models with the smallest electrode and it is not higher than 4%.

Now let us analyse the results obtained with different FDM formulations. The graph of the analytical solution is kept as a reference in all plots of the centre-line potential distribution of the sphere. The results of different resolutions of FDM centre-node formulation with 1 voxel electrode are plotted in Fig. 9.

In Fig. 9 it can be seen that increasing the resolution also increases the potential on the electrodes. This follows directly from the fact that by increasing the resolution the electrode size is decreased since it still takes up one voxel. The last points of the FDM lines are outside the sphere surface because an additional voxel was added to the sphere surface as electrode. Potential value of the last point is taken from the centre of the electrode voxel.

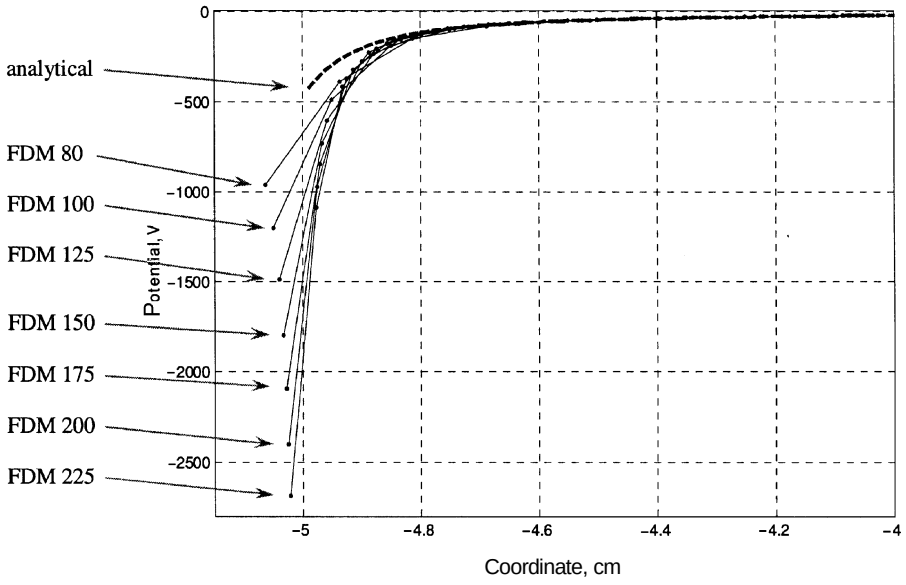

Fig. 9. FDM centre-voxel formulation used with increasing resolutions from 80 to 225 voxels in *x*, *y* and *z* direction of the sphere; the electrode corresponds to one voxel.

In Fig. 10 it can be seen that the corner-voxel formulation correlates much better with analytical solution near the surface of the sphere where the electrode is positioned. Note that the vertical scaling is changed to accomodate the graphs better. Once again, potential increases as the size of the 1 voxel electrode decreases with increasing resolution. In this plot the whole voxel of the electrode resides outside the sphere. We see almost horizontal lines and very little change in potential inside the last voxel designated to the electrode. That is caused by very high conductivity of the electrode.

With fixed electrode size the results are next plotted using different resolutions (Figs. 11 to 13). For the FDM formulations different electrode shapes are used as shown in Fig. 3.

The vertical scaling in the last two figures has been held the same to provide better comparison. Neither of the two FDM formulations can be meaningfully compared to the analytical solution because in the latter the electrodes are modelled as point electrodes. The analytical solution is shown for reference. The results of each of the FDM systems seem to be gathered around a small area or converged. The corner-voxel FDM results (Fig. 12) have smaller potential values at the electrode. This is due to the fact that it uses more connections to the surface than in the centre-voxel formulation and thus effectively distributes the current into the system through a wider contact surface.

Next, the results of both FDM systems in the $r = 1$ mm electrode case are compared with the FEM solution (Fig. 13). Only the highest resolution from both FDM systems is plotted to provide clean straightforward comparison.

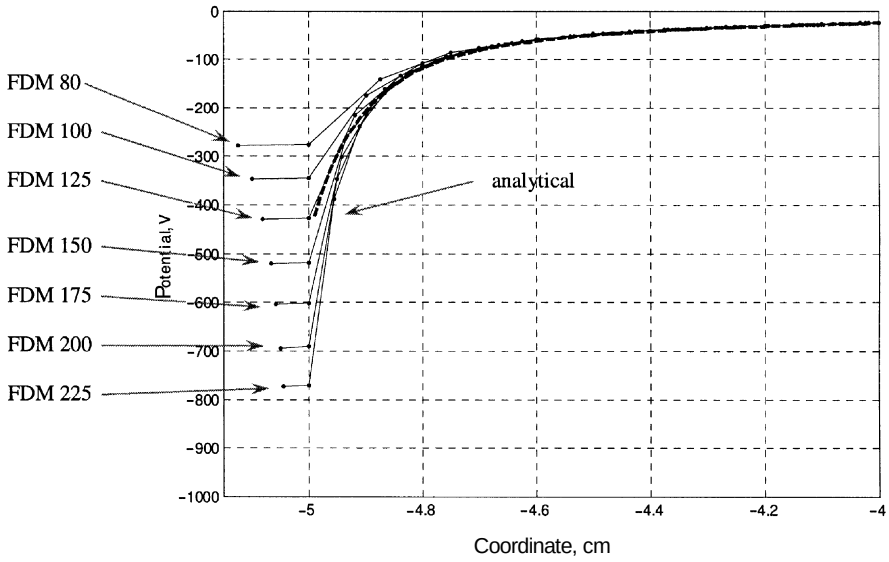

Fig. 10. FDM corner-voxel formulation used with increasing resolutions from 80 to 225 voxels in *x*, *y* and *z* direction of the sphere; the electrode corresponds to one voxel.

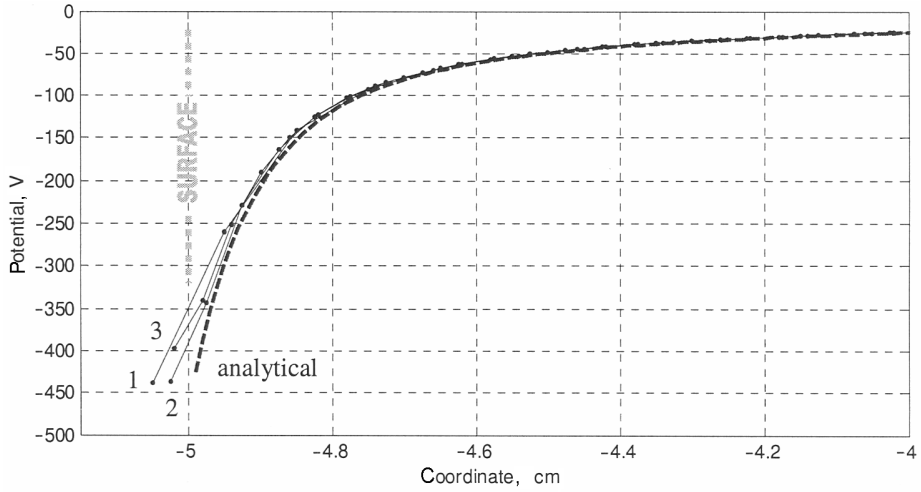

Fig. 11. FDM centre-voxel formulation compared with the analytical solution; electrode size is fixed at $r = 1$ mm; the FDM formulation used electrodes composed of: 1) 4 voxels, resolution 100; 2) 12 voxels, resolution 200; 3) 21 voxels, resolution 250 voxels (middle line of the three solid lines).

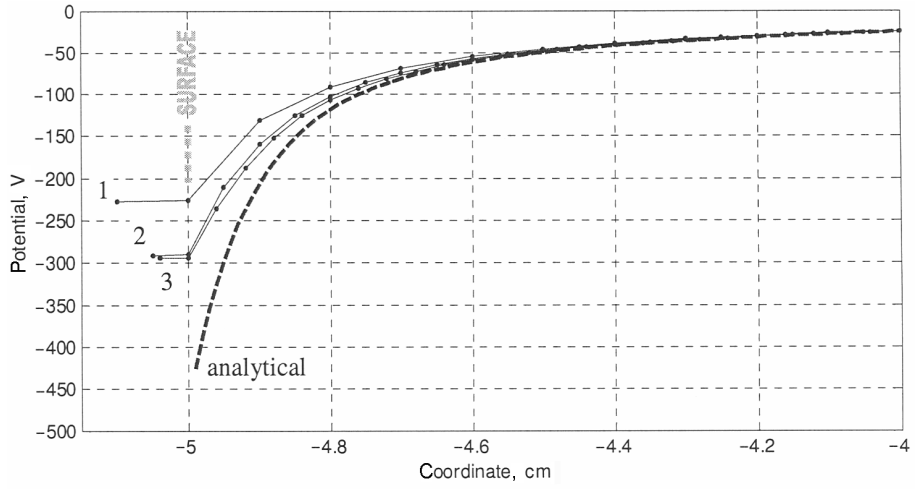

Fig. 12. FDM corner-voxel formulation compared with the analytical solution; electrode size fixed at $r = 1$ mm; the FDM formulation used electrodes composed of: 1) 4 voxels, resolution 100; 2) 12 voxels, resolution 200 (middle line of the three solid lines); 3) 21 voxels, resolution 250 voxels.

FEM uses higher density mesh near the electrode and therefore minimizes discretization errors. FEM mesh is also able to present the shape of the circular electrode more accurately.

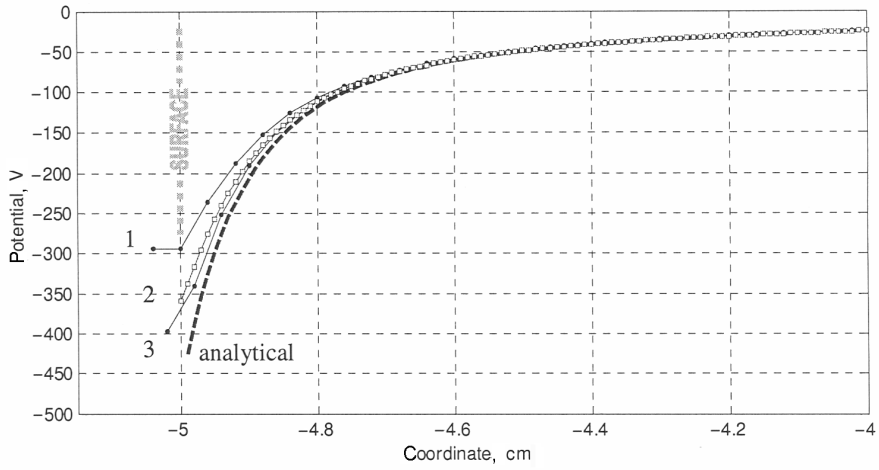

Fig. 13. Comparison of the modelling systems with r = 1 mm electrode: 1) FDM corner-voxel form; 2) FEM (r = 1 mm circular electrode); 3) FDM centre-voxel form; FDM formulations used electrodes composed of 21 voxels and resolution was 250 voxels.

Next we analyse analytical and FDM results for the three-layer spherical head model (Fig. 14).

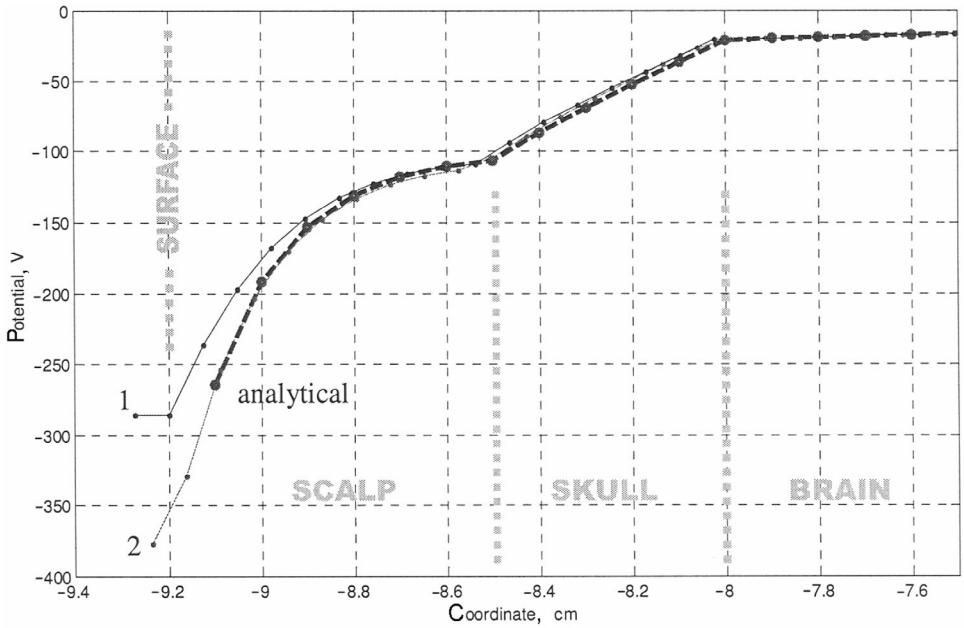

Fig. 14. Potential distribution near the electrode in a three-layer spherical head model; analytical solution is compared to the FDM corner-voxel formulation (1) and FDM center-voxel formulation (2).

Figure 14 shows the results from the FDM formulations with the highest resolution of 250 voxels in *x*, *y* and *z* direction and electrode area with 21 voxels (see Fig. 3). The analytical solution and centre-voxel formulation of FDM seem to have very good correlation. The exact match at the last 4–5 mm from the surface is probably an accidental coincidence, because the analytical solution should ideally represent the field of an infinitely small electrode while the real electrode has a radius of 1 mm. The most interesting is the skull area, where both FDM formulations are close to the analytical solution. When observed closely, centre-voxel formulation seems to cover the tissue interfaces (scalp-skull and skull-brain interfaces) more smoothly. This is due to the way it describes the connections between mesh nodes. Centre-voxel FDM formulation uses conductivity averaging between nodes that lay in neighbouring voxels. Corner-voxel formulation of FDM has sharper edges in the solution and it can also be seen in Fig. 14 (particularly near the skull–brain interface).

To understand how the differences observed in Fig. 14 are distributed inside the 3-dimentional sphere, the potentials are imaged on a slice through the middle of the sphere. Figure 15 illustrates the results of FDM corner-voxel formulation for reference. Figure 16a shows the areas of difference of the analytical results and FDM center-voxel form. Figure 16b shows the areas of difference of the analytical results and FDM corner-voxel form. Figure 17 shows the difference between the two FDM formulations.

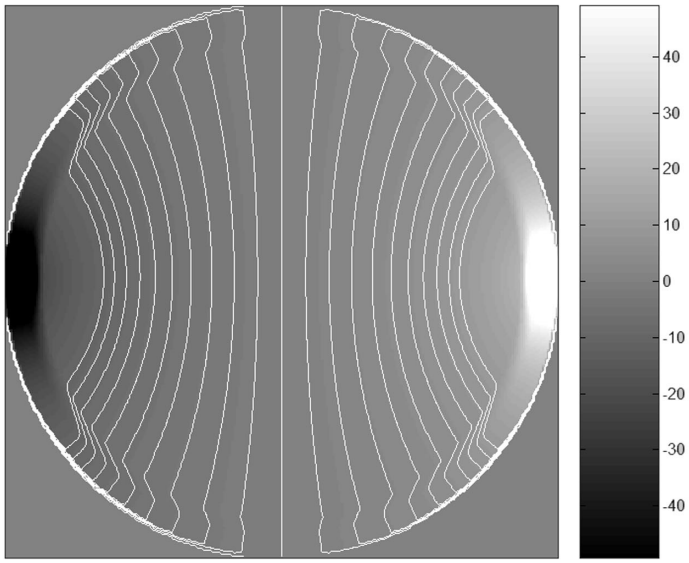

Fig. 15. Potential distribution in FDM corner-voxel formulation of the three-layer spherical head model; selected brightness contour-lines are added for better illustration of the field.

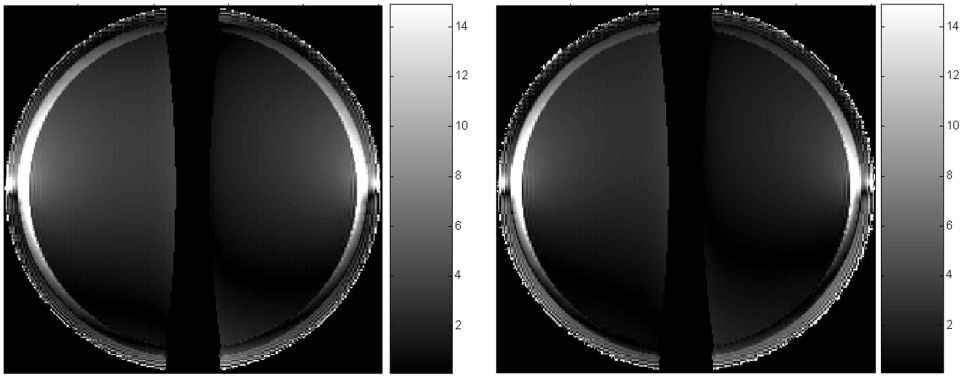

(a) (b)

Fig. 16. Areas of difference between analytical and FDM centre-voxel formulation (a) and analytical compared to FDM corner-voxel formulation (b); brightness shows calculated potential differences in percentages.

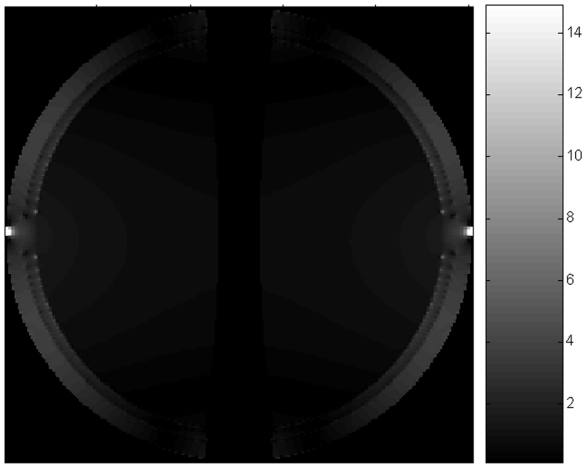

Fig. 17. Areas of difference between two FDM formulations; brightness shows calculated potential differences in percentages.

On these figures the biggest difference is at the electrode location with a value of 25% between the two FDM formulations (Figs. 14 and 17). Other areas did not exhibit differences above 15% (15% was therefore chosen as the brightest colour for Figs. 16 and 17). The centre area of the sphere, where potential values are negligibly small, was omitted from the difference plots. In Fig. 16 the two FDM formulations differ from the analytical solution in a similar way, because both FDM formulations used the same discretized model for grid generation. The area near the electrodes is most problematic and the differences in the skull area are also visible (in Fig. 16 shown as brighter band). The errors in the skull area are

arising from discretization, where the nodes of the FDM formulations did not happen to be at the exact boundary of the skull. In other areas, the differences between the FDM formulations and analytical solution did not exceed 5%. The two FDM methods differ very little from each other (less than 3%) except near the electrode (Fig. 17).

4. DISCUSSION

Looking at Fig. 3 we notice, that the shapes and surface areas of FDM and FEM implementations of electrodes do not match exactly. Still, with higher resolution (more voxels for electrode in FDM) it is possible to obtain a better shape and surface area match between the electrodes of FDM and FEM. Generally, most errors of numerical methods appear where discretization of the object is too sparse to accurately present the sharp changes of the calculated parameter (electric potential in our case). In impedance measurement this happens most often on the electrode interface with the object (tissue). Although other areas in the object can also exhibit very sharp differences in conductivity, the electrode interface remains to be the highest source of errors because of the high current density. In this study we are demonstrating the performance of FDM in possibly the worst scenario.

When using the analytical model extensively and studying also current densities within the model we noticed that the values obtained close to the surface of the sphere were not consistent. The analytical formula consists of a series of terms, which should be summed up to an infinite number of terms. When the number of terms was increased to reasonable maximum, the smoothness of current densities near the surface improved but was still far from the expected (smooth) distribution. When solving the current densities within a model with a 9.2 cm outer radius, the fluctuations in the current density extended from the surface to the depth of 2 mm. Therefore, also considering the potentials we cannot consider the analytical solution (with the accuracy applied) very reliable in the 2 mm proximity of the sphere surface.

As can be seen in Figs. 9, 10, 13 and 14, the same electrode surface in the two FDM formulations produces higher electrode potentials in the centre-voxel formulation. This might follow from the fact that when using one voxel electrodes, the centre-voxel formulation uses 1 node to enter the current into the subject instead of 4 (as in corner-voxel formulation). The centre-voxel FDM has effectively smaller electrode area and therefore needs more potential to produce the same current. These effects can be observed both in the homogeneous sphere model (Fig. 13) and in the three-layer model (Fig. 14). We therefore conclude that using few elements for the electrode does not produce consistent results with the FDM formulations near the electrode. This aspect of FDM modelling has to be investigated further and measures have to be taken to dramatically increase the number of voxels used for FDM-modelling of the electrodes. When absolute

values of the potential at the current-generation electrodes is not important, then both FDM formulations seem to give quite usable potential distribution inside the object that is consistent with the results of the analytical solution and FEM.

When modelling impedance measurement with the 4-electrode system (that uses separate electrodes for current insertion and voltage pick-up), the inaccuracies near the current insertion electrodes are not so important. The potential field inside the test object, starting from a short distance from excitation electrodes is accurate to within 3%. When sharp tissue boundaries are encountered, the FDM formulations can exhibit higher errors due to discretization. Differences as high as 15% were observed in the skull region near the electrode (Fig. 16). These discretization errors are assumed to be possible to minimize when higher resolutions of the FDM mesh are used.

Validity and usefullness of the results presented here depend on the applications. For lead sensitivity estimation, the potential on the model surface is not important. The lead sensitivity field equals to the current density field in the model and that has not been discussed here.

However, to make the potentials, calculated with different discretization methods, comparable, one must assert that the electrodes are large enough as compared to the discretization of the model. This brings up the question, what is a large enough electrode and what actually is gained using only one node as the source and the sink. For sensitivity mapping via the lead field theory there definitely is a reason for it, but to simulate actual measurement of a bioelectric phenomena it is of no purpose. Thus, a detailed study of the electrode size in the applied methods is needed.

Although FEM usually gives good results for complex problems, FDM is still needed in cases where proper meshing for FEM might become a problem. These cases include biological objects, where often the object is not described by surfaces but by discrete volume elements. FDM provides also a fast method for solving electric fields in biological media, where a multitude of models of the object are used. For example, in dynamic situations, where every frame of a moving object would have to be separately meshed in the FEM case.

The accuracy of the FDM on the electrode could be increased with local increasing of the FDM mesh resolution. FDM mesh density can also be increased near sharp boundaries that are close to the electrode (where higher signal change is expected). Implementing those features to the FDM solver, it would become a fast, accurate and robust tool for solving electric field problems.

REFERENCES

1. Malmivuo, J. and Plonsey, R. *Bioelectromagnetism: Principles and Applications of Bioelectric and Biomagnetic Fields*. Oxford University Press, USA, 1995.
2. Plonsey, R. and Barr, R. C. *Bioelectricity: A Quantitative Approach*. Kluwer Academic, New York, 2000.
3. Grimnes, S. and Martinsen, O. G. *Bioimpedance and Bioelectricity Basics*. Academic Press, London, 2000

4. Holder, D. S. *Electrical Impedance Tomography: Methods, History and Applications*. Institute of Physics Publishing, Philadelphia, 2005.
5. Tidswell, T., Gibson, A., Bayford, R. H. and Holder, D. S. Three-dimensional electrical impedance tomography of human brain activity. *NeuroImage*, 2001, **13**, 283–294.
6. Bagshaw, A. P., Liston, A. D., Bayford, R. H., Tizzard, A., Gibson, A. P., Tidswell, A. T., Sparkes, M. K., Dehghani, H., Binnie, C. D. and Holder, D. S. Electrical impedance tomography of human brain function using reconstruction algorithms based on the finite element method. *NeuroImage*, 2003, **20**, 752–764.
7. Burik, M. J. and Peters, M. J. Estimation of the electric conductivity from scalp measurements: feasibility and application to source localization. *Clin. Neurophys.*, 2000, **111**, 1524–1531.
8. Kauppinen, P., Hyttinen, J. and Malmivuo, J. Sensitivity distribution simulations of impedance tomography electrode combinations. *Internat. J. Bioelectromagn.*, 2005, **7**, 344–347.
9. Laarne, P., Eskola, H., Hyttinen, J., Suihko, V. and Malmivuo, J. Validation of a detailed model of the electrical fields in the brain. *J. Med. Eng. Technol.*, 1995, **19**, 84–87.
10. Oostenveld, R. and Oostendorp, T. F. Validating the boundary element method for forward and inverse EEG computations in the presence of a hole in the skull. *Human Brain Mapping*, 2002, **17**, 179–192.
11. Mejis, J. W., Peters, M. J. and Van Oosterom, A. On the numerical accuracy of the boundary element method. *IEEE Trans. Biomed. Eng.*, 1989, **36**, 1038–1049.
12. Reddy, J. N. *An Introduction to the Finite Element Method*. McGraw-Hill, New York, 2005.
13. Sachse, F. B. *Computational Cardiology: Modeling of Anatomy, Electrophysiology, and Mechanics*. Springer, Berlin, 2004.
14. Rush, S. and Drisscoll, D. A. EEG electrode sensitivity – an application of reciprocity. *IEEE Trans. Biomed. Eng.*, 1969, **16**, 15–23.
15. Laarne, P. *Implementation of a Realistic Conductivity Model for the Head*. Tampere University of Technology Publications, Tampere, 2000.
16. Oostendorp, T. F., Delbeke, J. and Stegeman, D. F. The conductivity of the human skull: results of in vivo and in vitro measurements. *IEEE Trans. Biomed. Eng.*, 2000, **47**, 1487–1492.
17. Munck, J. C. and Peters, M. A fast method to compute the potential in the multisphere model. *IEEE Trans. Biomed. Eng.*, 1993, **40**, 1166–1174.
18. Cuffin, B. N. Eccentric spheres models of the head. *IEEE Trans. Biomed. Eng.*, 1991, **38**, 871–878.
19. De Munck, J. C. The potential distribution in an anisotropic spheroidal volume conductor. *J. Appl. Phys.*, 1988, **64**, 464–470.
20. Zhou, H. and Van Oosterom, A. Computation of the potential distribution in a four-layer anisotropic concentric spherical volume conductor. *IEEE Trans. Biomed. Eng.*, 1992, **39**, 154–158.
21. Haataja, J., Käpyaho, J. and Rahola, K. *Numeeriset menetelmät*. CSC-Tieteellinen laskenta Oy, Yliopistopaino, Finland, 1993.
22. Bronzino, J. D. (ed.). *The Biomedical Engineering Handbook* (p. 162–172). CRC Press, Florida, 1995.
23. Nocedal, J. and Wright, S. *Numerical Optimization*. Springer, New York, 2000.
24. Siddiqi, A. H. *Applied Functional Analysis, Numerical Methods, Wavelet Methods, and Image Processing*. Marcel Dekker, New York, 2004.
25. Hyttinen, J. *Development Of Regional Aimed ECG Leads Especially For Myocardial Ischemia Diagnosis*. Tampere University of Technology publications 138, Tampere, 1994.
26. Kauppinen, P., Hyttinen, J. and Malmivuo, J. A software implementation for detailed volume conductor modelling in electrophysiology using finite difference method. *Comput. Meth. Progr. Bio.*, 1999, **58**, 191–203.

Numbriliste meetodite täpsus staatiliste ja kvaasistaatiliste elektriväljade arvutamisel

Rauno Gordon, Tuukka Arola, Katrina Wendel, Outi Ryynanen
ja Jari Hyttinen

On uuritud numbriliste meetodite FDM ja FEM täpsust elektriväljade arvutamisel sfäärilises elektrijuhis. On kirjeldatud kahte erinevat FDM-i formuleeringut. Esimeses neist asetsevad FDM-i võre sõlmed kuubikukujuliste ruumielementide nurkades, teises keskmetes. Nende kahe formuleeringu tulemusi on võrreldud analüütilise meetodi ja FEM-i tulemusega, arvutades elektrivälja homogeenses ja kolmekihilises sfäärilise pea mudelis. Elektroodid on asetatud sfäärilise mudeli pinnale kahel vastaspoolel. FDM-i formuleeringute tulemused erinevad objektide seesmistes osades kuni 5%. Kolmekihilise mudeli sees kasvavad aga vead kahe koe eralduspindadel kuni 15%-ni kohtades, mis on elektroodidele kõige lähemal. Erinevate arvutusmeetodite tulemuste erinevused elektroodide juures ulatuvad 25%-ni.